Recurrence networks from multivariate signals for uncovering dynamic transitions of horizontal oil-water stratified flows

Zhong-Ke Gao[1,2,3], Xin-Wang Zhang[1], Ning-De Jin[1], Reik V. Donner[3], Norbert Marwan[3] and Jürgen Kurths[2,3,4]

[1] *School of Electrical Engineering and Automation, Tianjin University - Tianjin 300072, China*
[2] *Department of Physics, Humboldt University - Berlin 12489, Germany, EU*
[3] *Potsdam Institute for Climate Impact Research - Potsdam 14473, Germany, EU*
[4] *Institute for Complex Systems and Mathematical Biology, University of Aberdeen - Aberdeen AB24 3UE, UK, EU*

Abstract – Characterizing the mechanism of drop formation at the interface of horizontal oil-water stratified flows is a fundamental problem eliciting a great deal of attention from different disciplines. We experimentally and theoretically investigate the formation and transition of horizontal oil-water stratified flows. We design a new multi-sector conductance sensor and measure multivariate signals from two different stratified flow patterns. Using the Adaptive Optimal Kernel Time-Frequency Representation (AOK TFR) we first characterize the flow behavior from an energy and frequency point of view. Then, we infer multivariate recurrence networks from the experimental data and investigate the cross-transitivity for each constructed network. We find that the cross-transitivity allows quantitatively uncovering the flow behavior when the stratified flow evolves from a stable state to an unstable one and recovers deeper insights into the mechanism governing the formation of droplets at the interface of stratified flows, a task that existing methods based on AOK TFR fail to work. These findings present a first step towards an improved understanding of the dynamic mechanism leading to the transition of horizontal oil-water stratified flows from a complex-network perspective.

Introduction. – Horizontal oil-water two-phase flow is frequently encountered in many industrial processes and the interest in them has greatly increased recently mainly due to the petroleum industry [1,2]. When oil and water flow in a horizontal or slightly inclined pipe, there exist particular flow conditions for which the two immiscible phases are separated from each other by a continuous smooth or wavy interface. For a fixed water flow rate, when the oil flow rate is low, the interface is smooth or may be rippled by very small capillary waves, *i.e.*, stratified (ST) flow pattern occurs. With an increase of the oil flow rate, interfacial waves gradually appear. When the oil flow rate is high, droplets can be formed from the interfacial waves, *i.e.*, an onset of a stratified flow with mixing at the interface (ST&MI) pattern is formed. Note that the horizontal oil-water dispersed flow patterns, including a dispersion of oil in water and water flow pattern and a dispersion of water in oil and oil in water flow pattern, evolve

from the ST&MI flow pattern. The investigation on the dynamic transitions from a ST flow pattern to a ST&MI flow pattern can yield deeper insights into the mechanism governing the formation of droplets, which is very crucial for understanding the formation and transition of horizontal oil-water dispersed flow patterns. Therefore, the study of ST flow and ST&MI flow is of paramount importance. Distinct horizontal oil-water flow patterns have been observed [3,4] and the characterization of oil-water flows has attracted much attention from physical and chemical research fields. Numerical simulations [5], wavelet multiresolution technique [2] and theoretical models [6,7] have been employed to study experimental horizontal oil-water two-phase flows. But compared to the study of gas-liquid flows, works particularly dedicated to the investigation of horizontal stratified flows are quite limited. In addition, the mechanism of drop formation at the interface of horizontal oil-water stratified flows is still elusive. Therefore, it

becomes quite important and necessary to develop a new and effective tool to quantitatively uncover the mechanisms leading to the formation and transition of horizontal oil-water stratified flows from experimental measurements.

Complex-network theory has provided an increasingly challenging framework for the study of complex systems from different research fields [8–15]. Charting the interactions between system components, abstracted as nodes and edges, has allowed us to represent a complex system as a complex network and then assess the system in terms of network theory. Recently, complex-network methods applied to time series analysis have proven great potential for characterizing important properties of complex dynamical systems [16–30]. In particular, the recurrence network technique [25–30] has established itself as a powerful tool for quantitatively and geometrically characterizing complex dynamical systems and time series. We recently have used recurrence networks to successfully identify five different horizontal oil-water flow patterns [31].

In this letter, we aim to experimentally and theoretically study the mechanisms leading to the formation and transition of horizontal oil-water stratified flows. We design a new multi-sector conductance sensor and systematically carry out horizontal oil-water two-phase flow experiments for measuring multivariate signals from ST flow pattern and ST&MI flow pattern. Utilizing the Adaptive Optimal Kernel Time-Frequency Representation (AOK TFR), we first investigate the flow behaviors from different local measured signals. We find that the local flow behaviors of ST flow patterns and ST&MI flow patterns are distinct in the sense that their energy and frequency distributions are different, but the energy and frequency distributions are not very sensitive to the transitions of flow conditions and hence the AOK TFR method does not allow uncovering the mechanism governing the formation of drops at the interface of stratified flows. In this regard, we resort to the multivariate recurrence network to investigate the horizontal oil-water stratified flows. We find that the inferred multivariate recurrence networks exhibit the topological structure of "network of networks", which can be quantitatively assessed by the cross-transitivity. Our results suggest that the cross-transitivity allows quantitatively uncovering the flow behavior when the stratified flow evolves from a stable state to an unstable state and can yield deeper insights into the mechanism governing the formation of drops at the interface of stratified flows, a task that existing methods based on AOK TFR fail to work.

Experiments and data acquisition. – We carry out a horizontal oil-water two-phase flow experiment in a 20-mm-inner-diameter pipe in a multiphase flow loop at Tianjin University. The main sensor is our newly designed four-sector conductance sensor (fig. 1(a)), which enables to measure the local flow behavior of horizontal oil-water flows. It consists of eight alloy titanium concave electrodes axially separated and flush mounted on the in-
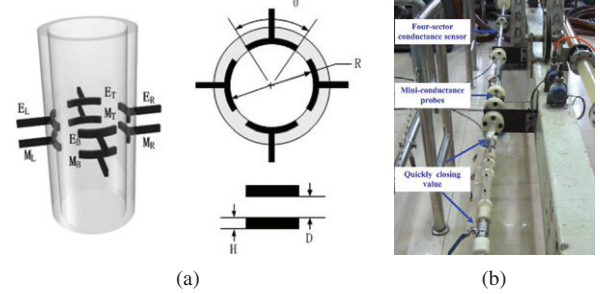

Fig. 1: (Color online) (a) The four-sector conductance sensor: E_T, E_R, E_B, E_L are the exciting electrodes, and M_T, M_R, M_B, M_L are the measuring electrodes, respectively, θ is the exciting and measuring electrode angle, H is the electrode height, R is the inner pipe radius, and D the distance between the exciting and the measuring electrode; (b) experimental flow loop facility.
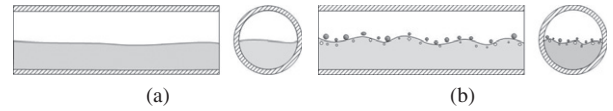

Fig. 2: Horizontal oil-water stratified flow patterns. (a) ST flow; (b) ST&MI flow.

side wall of the flowing pipe. Figure 1(b) shows our experimental flow loop facility. The experimental media are tap water and No.15 industry white oil. In the experiment, when the water and oil flow rates reach a pre-defined ratio, a certain flow condition is obtained and conductance fluctuating signals are then acquired from the four-sector conductance sensor. The oil and water superficial velocities are both in the range of 0.1–3 m/s. The sampling frequency is 4000 Hz and the measuring time for one measurement is 30 s. In the experiment, when the oil and water flow rates are low, the flow pattern is ST. With an increase of the flow rates, interfacial waves between oil phase and water phase gradually appear and are initially long. With a further increase of the flow rates, these waves will become disturbed. Along the interfacial waves, one or more droplets of one phase will appear in the other continuous phase, *i.e.*, the oil-water flows evolve from a ST flow to a ST&MI flow (fig. 2). The flow signals from the four-sector conductance sensor corresponding to ST and ST&MI flow patterns are shown in fig. 3.

Time-frequency representation of oil-water stratified flows. – Adaptive optimal kernel time-frequency representation (AOK TFR), which has been widely applied to analyze non-stationary signals, performs a mapping from the time domain to the time-frequency domain. More details about the AOK TFR method are given in ref. [32]. In fig. 4 and fig. 5 we show the AOK TFR results of the horizontal oil-water ST flow pattern and the ST&MI flow pattern, respectively, where the spectra represent the power spectral density of the original signals. For the ST flow, the upper part of the
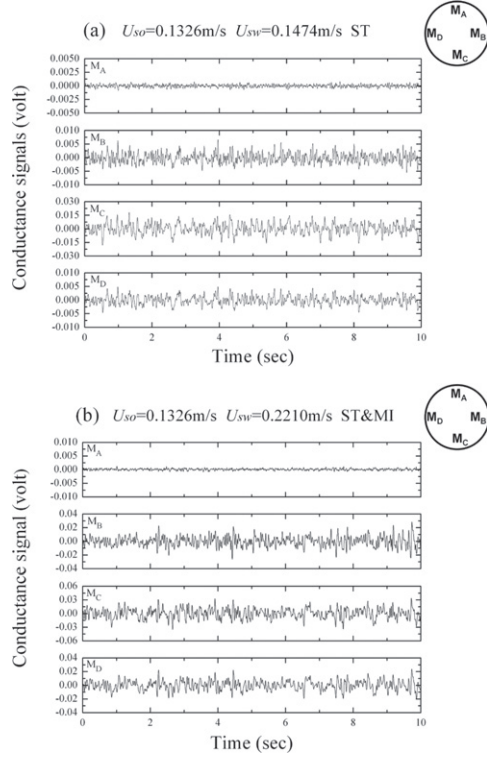
Fig. 3: The signals from the four-sector conductance sensor for two different horizontal oil-water stratified flow patterns: (a) ST flow; (b) ST&MI flow, where U_{so} and U_{sw} represent the oil superficial velocity and the water superficial velocity, respectively.

Fig. 4: (Color online) AOK TFR for a typical horizontal oil-water ST flow pattern ($U_{sw} = 0.1105$ m/s, $U_{so} = 0.1326$ m/s). (a) M_A signals; (b) M_B signals; (c) M_C signals; (d) M_D signals.

Fig. 5: (Color online) AOK TFR for a typical horizontal oil-water ST&MI flow pattern ($U_{sw} = 0.3684$ m/s, $U_{so} = 0.1326$ m/s). (a) M_A signals; (b) M_B signals; (c) M_C signals; (d) M_D signals.

horizontal pipe is the continuous oil phase and the bottom part the continuous water phase. The ST flow pattern can be characterized by a smooth oil-water interface with no droplets and only small waves (fig. 2(a)). As can be seen in fig. 4(a), the frequency of the continuous oil phase in the upper part of the pipe is in the range of 0–60 Hz, but its energy is very low. In the bottom part, due to effects of turbulence, the frequency of the continuous water phase is in the range of 0–40 Hz and its energy becomes higher compared to that of the continuous oil phase (fig. 4(c)). The AOK TFR results of M_B and M_D signals are very similar (fig. 4(b) and (d)), and the frequencies are both in the range of 0–30 Hz and the energies are higher than in the continuous oil phase but lower than in the continuous water phase, reflecting the flow behavior of interfacial waves. With an increase of the flow rate, the turbulence energy increases, resulting in the appearance of few oil and water droplets around the interface and then a ST&MI flow pattern occurs. Similar to the ST flow pattern, the AOK TFR of the upper part of the ST&MI flow pattern still reflects the flow behavior of the continuous oil phase, exhibiting features in wide frequency and low energy (fig. 5(a)). Different to the ST flow pattern, the frequency and energy of the right and left part ST&MI flow pattern become obviously larger than that of the ST flow pattern (fig. 5(b), (d) and
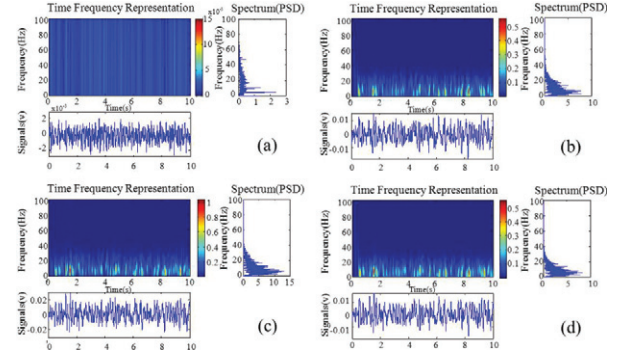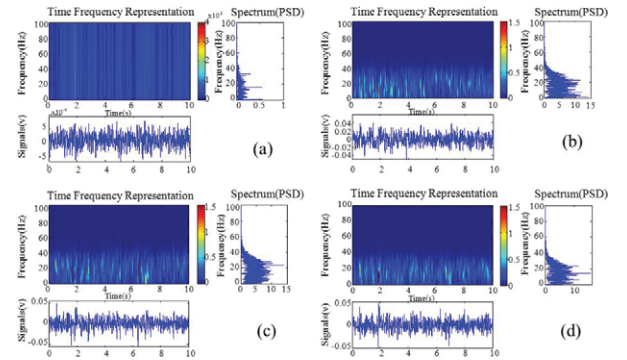
fig. 4(b), (d)), reflecting the increase in the amplitudes of the interfacial waves and also the movements of droplets along the interfacial waves. In addition, from fig. 5(c) and fig. 4(c) we can see that the energy of the bottom part of ST&MI flow also increases compared to ST flow, indicating the increase of the turbulence energy induced by increasing water flow rate.

From the analysis above, we can see that the local flow behaviors of typical ST flow pattern and ST&MI flow pattern are distinct in the sense that their energy and frequency distributions are different. But it should be pointed out that the energy and frequency distributions actually are not very sensitive to the transitions of flow conditions. For example, when we fix the water flow rate at 0.1326 m/s, and increase the oil flow rate from 0.1105 m/s to 0.1474 m/s we see the formation and transition of a ST flow pattern, and then proceed to increase the oil flow rate from 0.1474 m/s to 0.2210 m/s we observe the formation and transition of ST&MI flow pattern. We find that the distributions of AOK TFR present very similar distributions in the transition from ST to ST&MI flow pattern, *e.g.*, when the water flow rate increases from 0.1474 m/s to 0.2210 m/s, which cannot be used to uncover

details of the transitions of stratified flow patterns. In this regard, the AOK TFR method does not allow uncovering the mechanism governing the formation of drops at the interface of stratified flows. It is thus necessary to develop a more efficient approach to uncover the mechanism leading to the formation of ST and ST&MI flow patterns. Therefore, in the next section we will resort to the multivariate recurrence networks and demonstrate its power in characterizing horizontal oil-water stratified flows.

Multivariate recurrence network analysis of stratified flows. – Multivariate time series (*e.g.*, our experimental signals M_A, M_B, M_C and M_D) can be embedded into the same phase space by using a suitable m-dimensional embedding with a proper time delay τ. Given a certain threshold ε and a certain distance norm $\| \cdot \|$, we can then get recurrence relationships between any two space vectors in this phase space. In particular, for vectors that come from the same time series (such as M_A),

$$\overrightarrow{M_A}(t) = (M_A(t), M_A(t + \tau), \dots, M_A(t + (m-1)\tau)), \quad (1)$$
$$t = 1, 2, \dots, N + m - 1,$$

we get the auto-recurrence matrix R^A as follows:

$$R_{ij}^A = \Theta(\varepsilon_A - \| \overrightarrow{M_A}(i) - \overrightarrow{M_A}(j) \|), \qquad (2)$$

and as for vectors from different time series (such as M_A and M_B), we get the cross-recurrence matrix $R_{cross}^{AB}(i,j)$ as

$$CR_{ij}^{AB} = \Theta(\varepsilon_{AB} - \| \overrightarrow{M_A}(i) - \overrightarrow{M_B}(j) \|), \qquad (3)$$

where $\Theta(\cdot)$ is the Heaviside function $\Theta(x) = \{1 \mid x > 0; 0 \mid x \leq 0\}$. The embedding dimension m and delay time τ should be properly selected to reconstruct phase space and we use the FNN [33] method and the C-C [34] method to determine m and τ, respectively. Combining the cross- and auto-recurrence matrix, we obtain a multivariate recurrence matrix IR

$$IR = \begin{pmatrix} R^A & CR^{AB} & CR^{AC} & CR^{AD} \\ CR^{BA} & R^B & CR^{BC} & CR^{BD} \\ CR^{CA} & CR^{CB} & R^C & CR^{CD} \\ CR^{DA} & CR^{DB} & CR^{DC} & R^D \end{pmatrix}. \quad (4)$$

In order to consider the IR as a network of networks, the cross-recurrences should be lower than the auto-recurrences

$$\frac{1}{N(N-1)} \sum_{i \neq j} R_{ij}^A > \frac{1}{N_A N_B} \sum_{i,j} CR_{ij}^{AB} \qquad (5)$$

According to ref. [29], we fix the auto- and cross recurrence rate at 0.03 and 0.02, respectively. Note that, the recurrence rate reflects the edge density of a recurrence network. For a time series, there exists a one-to-one mapping between the recurrence rate and the recurrence threshold, and one recurrence rate exclusively corresponds to one recurrence threshold. For different time series, the same

recurrence rate can generate different recurrence thresholds. In particular, we determine the thresholds for auto- (cross-) recurrence networks in terms of the same fixed auto- (cross-) recurrence rate, and the recurrence thresholds for different auto- (cross-) recurrence networks are different. Therefore, the thresholds in the multivariate recurrence matrix IR can be different. Consequently, we obtain a multivariate recurrence network by interpreting the multivariate recurrence matrix as a network adjacent matrix. More details about the recurrence network and recurrence analysis are in refs. [26,35].

Four signals measured from one flow condition are mapped into a multivariate recurrence network. For each generated multivariate recurrence network, there exist four subnetworks, denoted as subnetwork A, B, C, D, resulting from the four different sector signals M_A, M_B, M_C and M_D, respectively. In order to characterize the local and cross property between subnetworks, we use the recently proposed cross-transitivity [29]. A cross-transitivity for subnetwork A to B can be defined as follows:

$$T^{AB} = \frac{\sum_{v \in A; p,q \in B} CR_{vp}^{AB} CR_{vq}^{AB} R_{pq}^B}{\sum_{v \in A; p,q \in B} CR_{vp}^{AB} CR_{vq}^{AB}} \qquad (6)$$

Actually, T^{AB}, as an analog to the canonical network transitivity [8], counts the number of "cross-triangles" over the number of "cross-triples". It is important to indicate that the cross-transitivity is not invariant under the permutation A $\leftrightarrow$ B, *i.e.*, $T^{AB} \neq T^{BA}$. Note that for two subnetworks A and B constructed from two coupled dynamic systems, if the coupling direction is A $\to$ B and the coupling is large enough, we can find a state $\overrightarrow{B}(k)$ in B, which is cross-recurrent to both $\overrightarrow{A}(i)$ and $\overrightarrow{A}(j)$, due to the coupling's diffusive nature and thus the tendency to "drag" the trajectory of B towards A. The resulting "cross-triangle" adds to the value of T^{BA} according to the definition of cross-transitivity. Therefore, we see that $T^{BA} > T^{AB}$ in case of a unidirectional coupling A $\to$ B and vice versa for the opposite coupling direction. We calculate the cross-transitivity between all pairs of subnetworks for each constructed network to investigate the flow behavior leading to the formation and transition of horizontal oil-water stratified flows. The number of data points for each signal entered the analysis is 120000. Note that, for each flow condition, we divide the four signals M_A, M_B, M_C, M_D, into six parts with equal length, *i.e.*, $M_A(i)$, $M_B(i)$, $M_C(i)$, $M_D(i)$, $i = 1, 2, 3, \dots, 6$. Then we construct the network and calculate the cross-transitivity for each part, and finally we obtain the ensemble mean and standard deviation of the cross-transitivity for the six parts. We show the cross-transitivity of all pairs of subnetworks for a multivariate recurrence network generated from the ST flow pattern (fig. 6(a)), and the ST&MI flow pattern (fig. 6(b)). We calculate the ensemble means and standard deviations (error bars) of the cross-transitivity for all flow conditions in the transitions from ST flow to ST&MI flow and present the results in fig. 7. For the ST
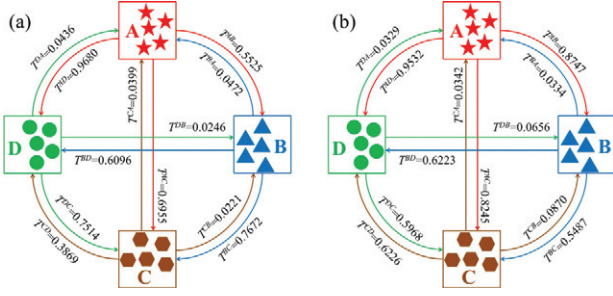
Fig. 6: (Color online) Cross-transitivity of all pairs of sub-networks for a multivariate recurrence network generated from (a) ST flow pattern (U_{so} = 0.1945 m/s, U_{sw} = 0.1105 m/s) and (b) ST&MI flow pattern (U_{so} = 0.1945 m/s, U_{sw} = 0.2216 m/s), where A, B, C, D represent different subnetworks.
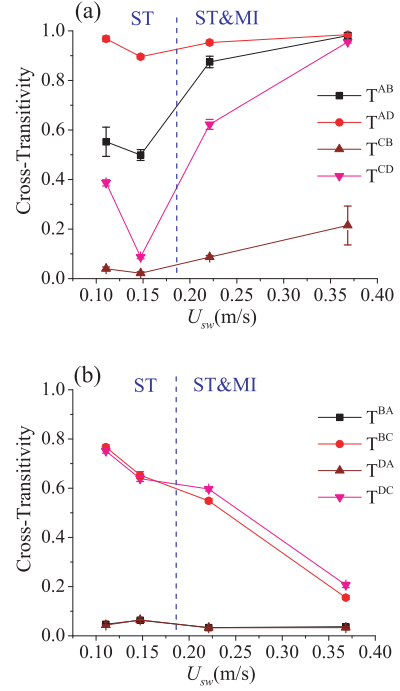

Fig. 7: (Color online) Cross-transitivity for the transitions from ST flow to ST&MI flow, where some error bars are smaller than the size of the symbols.

flow pattern $m = 3$, $\tau = 18$; for the ST&MI flow pattern $m = 3$, $\tau = 24$. As can be seen, the cross-transitivity is very sensitive to the transitions of flow conditions. Note that subnetwork A and C reflect the flow behavior of the upper and bottom part of the stratified flow, respectively, and subnetwork B and D reflect the flow behavior of the middle right and left part of the stratified flow, respectively. Since at the transition from ST flow to ST&MI flow interfacial waves occur at the middle part of the stratified flow, the cross-transitivity associated with subnetwork B and D can be targetedly used to uncover the mechanism governing the formation and transition of ST and ST&MI flow pattern. Specifically, the values of T^{AB}, T^{AD}, T^{CB}, T^{CD}, T^{BC}, T^{DC}, T^{BA}, T^{DA} for different stratified flow patterns are located in distinct regions, and when a transition from ST flow to ST&MI flow occurs, a sudden change of cross-transitivity will appear (fig. 7), which allows quantitatively distinguishing ST flow from ST&MI flow.

We now demonstrate how to investigate the mechanism leading to the formation of droplets at the oil-water interface in the transition from ST flow to ST&MI flow in terms of the network measure from multivariate recurrence networks. For a fixed oil flow rate, when the water flow rate is low, e.g., $U_{sw} = 0.1105$ m/s, the ST flow is in a stable state and there are no interfacial waves or there only exist interfacial waves of small amplitudes at the oil-water interface. With an increase of the water flow rate, e.g., $U_{sw} = 0.1474$ m/s, the amplitudes of the interfacial waves gradually increase and the turbulence of water phase also increases, but the interfacial waves are still stable and the wave amplitudes are not large enough to form droplets under this flow condition. Correspondingly, for ST flow pattern, as the water flow rate increases from 0.1105 m/s to 0.1474 m/s, the T^{BC} and T^{DC} gradually decrease, indicating the increase of the amplitudes of the stable interfacial waves (fig. 7). Note that the drag force resulting from the difference between the oil flow rate and the water flow rate will lead to an increase of the wave amplitudes and the deformation of interfacial waves, but the gravity and surface tension force tends to preserve the original interfacial wave shape. With a further increase of the water flow rate,

e.g., $U_{sw} = 0.2210$ m/s, the water phase moves at a higher flow rate than the oil phase and begins to undercut the oil layer until the breakage of droplets becomes possible, i.e., the onset of ST&MI flow pattern. It should be noted that the formation of droplets at the oil-water interface becomes possible only if the drag force exceeds the retaining force of surface tension. As can be seen in fig. 7(a), when the water flow rate is low and the interfacial waves are stable, the T^{AB}, T^{AD}, T^{CB}, T^{CD} gradually decrease with the increase of the water flow rate. When the water flow rate reaches to $U_{sw} = 0.2210$ m/s, a sudden change of cross-transitivity T^{AB}, T^{AD}, T^{CB}, T^{CD} occurs and then T^{AB}, T^{AD}, T^{CB}, T^{CD} will increase with an increasing water flow rate. This sudden change of cross-transitivity indicates that the interfacial waves have evolved from a stable state to an unstable state and the drag force has exceeded the surface tension and, consequently, droplets are formed from the unstable oil-water interface. In addition, as shown in fig. 7(b), the cross-transitivity T^{BC} and T^{DC} for the stable stratified flow (ST flow) are usually large, while for the unstable stratified flow (ST&MI flow) they are small, and the decrease of T^{BC} and T^{DC} suggests that the amplitudes of the interfacial waves gradually increase. When the water flow rate increases from 0.1474 m/s to 0.2210 m/s, T^{BC} decreases from 0.65 to 0.54 and T^{DC} decreases from 0.64 to 0.59, indicating that the amplitudes of the interfacial waves have reached a critical value for the formation of droplets. These interesting results suggest that the cross-transitivity, which is very sensitive to the amplitude of interfacial waves, can faithfully characterize

the flow behavior when the stratified flow evolves from a ST stable state to a ST&MI unstable state and can yield deeper insights into the mechanism governing the formation of drops at the interface of stratified flows, a task that existing methods based on AOK TFR fail to work.

Conclusions. – The problem of characterizing the formation and transition of horizontal oil-water stratified flows based on experimental measurements has been a challenge in the study of multiphase flow. We design a new multi-sector conductance sensor for measuring multivariate signals from ST flow and ST&MI flow. We exploit the framework of multivariate recurrence network to construct network from multivariate signals for different flow conditions and arrive at a result of "network of networks", which can be assessed by the network measures crosstransitivity. Our results suggest that the cross-transitivity can faithfully indicate the formation of droplets at the interface induced when the drag forces become greater than the surface tension force, and further allow quantitatively characterizing the flow behavior associated with the formation and transition of horizontal oil-water stratified flows, a task that existing methods based on AOK TFR fail to work. Due to the effectiveness and generality of the method, we expect it to be useful for broader applications in science and engineering.

$$* * *$$

REFERENCES

[1] Xu X. X., *J. Pet. Sci. Eng.*, **59** (2007) 43.
[2] Chakrabarti D. P., Das G. and Das P. K., *AIChE J.*, **52** (2006) 3668.
[3] Trallero J. L., Sarica C. and Brill J. P., *SPE Prod. Facil.*, **12** (1997) 165.
[4] Rodriguez O. M. H. and Oliemans R. V. A., *Int. J. Multiphase Flow*, **32** (2006) 323.
[5] Ng T. S., Lawrence C. J. and Hewitt G. F., *Int. J. Multiphase Flow*, **27** (2001) 1301.
[6] Al-Wahaibi T., Smith M. and Angeli P., *Chem. Eng. Sci.*, **62** (2007) 2929.
[7] Piela K., Ooms G. and Sengers J. V., *Phys. Rev. E*, **79** (2009) 021403.
[8] Newman M. E. J., *Phys. Rev. E*, **64** (2001) 016131.
[9] Boccaletti S., Latora V., Moreno Y., Chavez M. and Hwang D. U., *Phys. Rep.*, **424** (2006) 175.
[10] Huang L., Park K., Lai Y. C., Yang L. and Yang K. Q., *Phys. Rev. Lett.*, **97** (2006) 164101.
[11] Buldyrev S. V., Parshani R., Paul G., Stanley H. E. and Havlin S., *Nature*, **464** (2010) 1025.
[12] Schneider C. M., de Arcangelis L. and Herrmann H. J., *EPL*, **95** (2011) 16005.
[13] Ansmann G. and Lehnertz K., *Phys. Rev. E*, **84** (2011) 026103.
[14] Iwayama K., Hirata Y., Takahashi K., Watanabe K., Aihara K. and Suzuki H., *Sci. Rep.*, **2** (2012) 423.
[15] Gao J., Buldyrev S. V., Stanley H. E. and Havlin S., *Nat. Phys.*, **8** (2012) 40.
[16] Zhang J. and Small M., *Phys. Rev. Lett.*, **96** (2006) 238701.
[17] Yang Y. and Yang H. J., *Physica A*, **387** (2008) 1381.
[18] Lacasa L., Luque B., Ballesteros F., Luque J. and Nuño J. C., *Proc. Natl. Acad. Sci. U.S.A.*, **105** (2008) 4972.
[19] Shimada Y., Ikeguchi T. and Shigehara T., *Phys. Rev. Lett.*, **109** (2012) 158701.
[20] Campanharo A. S. L. O., Sirer M. I., Malmgren R. D., Ramos F. M. and Amaral L. A. N., *PLoS ONE*, **6** (2011) e23378.
[21] Gao Z. K. and Jin N. D., *Phys. Rev. E*, **79** (2009) 066303.
[22] Gao Z. K., Jin N. D., Wang W. X. and Lai Y. C., *Phys. Rev. E*, **82** (2010) 016210.
[23] Ghaffari H. O. and Young R. P., *EPL*, **98** (2012) 48003.
[24] Walker D. M., Tordesillas A., Nakamura T. and Tanizawa T., *Phys. Rev. E*, **87** (2013) 032203.
[25] Xu X., Zhang J. and Small M., *Proc. Natl. Acad. Sci. U.S.A.*, **105** (2008) 19601.
[26] Marwan N., Donges J. F., Zou Y., Donner R. V. and Kurths J., *Phys. Lett. A*, **373** (2009) 4246.
[27] Gao Z. K. and Jin N. D., *Chaos*, **19** (2009) 033137.
[28] Donner R. V., Zou Y., Donges J. F., Marwan N. and Kurths J., *New J. Phys.*, **12** (2010) 033025.
[29] Feldhoff J. H., Donner R. V., Donges J. F., Marwan N. and Kurths J., *Phys. Lett. A*, **376** (2012) 3504.
[30] Gao Z. K., Zhang X. W., Du M. and Jin N. D., *Phys. Lett. A*, **377** (2013) 457.
[31] Gao Z. K., Zhang X. W., Jin N. D., Marwan N. and Kurths J., *Phys. Rev. E*, **88** (2013) 032910.
[32] Jones D. L. and Baraniuk R. G., *IEEE Trans. Signal Process.*, **43** (1995) 2361.
[33] Kennel M. B., Brown R. and Abarbanel H. D. I., *Phys. Rev. A*, **45** (1992) 3403.
[34] Kim H. S., Eykholt R. and Salas J. D., *Physica D*, **127** (1999) 48.
[35] Marwan N., Romano M. C., Thiel M. and Kurths J., *Phys. Rep.*, **438** (2007) 237.